Journal of Organometallic Chemistry 693 (2008) 2732–2738

Contents lists available at ScienceDirect

Journal of Organometallic Chemistry

journal homepage: www.elsevier.com/locate/jorganchem

Disulfido iron–manganese carbonyl cluster complexes: Synthesis, structure, bonding and properties of the radical $CpFeMn_2(CO)_7(\mu_3\text{-}S_2)_2$

Richard D. Adams [a,*], Erin M. Boswell [a], Burjor Captain [a,1], Shaobin Miao [a], Chad Beddie [b], Charles Edwin Webster [b,2], Michael B. Hall [b], Naresh S. Dalal [c], Narpinder Kaur [c], David Zipse [c]

[a] Department of Chemistry and Biochemistry, University of South Carolina, Columbia, SC 29208, United States
[b] Department of Chemistry, Texas A&M University, College Station, TX 77843-3255, United States
[c] Department of Chemistry and Biochemistry and Center for Magnetic Resonance National High Magnetic Field Laboratory, Florida State University, Tallahassee, FL 32306-4390, United States

ARTICLE INFO

Article history:
Received 15 May 2008
Accepted 16 May 2008
Available online 29 May 2008

Keywords:
Manganese
Iron
Disulfido
Radical
Molecular orbitals

ABSTRACT

Two new compounds $CpFeMn_2(CO)_7(\mu_3\text{-}S_2)_2$ (**2**) and $Cp_3Fe_3Mn(CO)_4(\mu_3\text{-}S_2)_2(\mu_3\text{-}S)$ (**3**) were obtained by the treatment of $[CpFeMn(CO)_5(\mu_3\text{-}S_2)]_2$ (**1**) with CO at room temperature in the presence of room light. Compound **2** contains two triply bridging disulfido ligands on opposite sides of an open $FeMn_2$ triangular cluster. EPR and temperature-dependent magnetic susceptibility measurements show that it is paramagnetic with one unpaired electron per formula equivalent. The electronic structure of **2** was established by DFT and Fenske-Hall (FH) molecular orbital calculations which show that the unpaired electron occupies a low lying antibonding orbital that is located principally on the iron atom. The cyclic voltammogram of **2** exhibits one reversible one-electron oxidation wave at +0.34 V and one irreversible one-electron reduction wave at −0.66 V vs. Ag/AgCl. Compound **3** contains three iron atoms and one manganese atom with two triply bridging disulfido ligands and one triply bridging sulfido ligand and has no unpaired electrons. The molecular structures of compounds **2** and **3** were established by single crystal X-ray diffraction analyses.

© 2008 Elsevier B.V. All rights reserved.

1. Introduction

Transition metal complexes containing sulfido ligands present one of the most rich and varied fields of modern inorganic coordination chemistry [1]. Polynuclear metal–sulfur complexes exhibit a range of different structural types [2]. Mixed-metal sulfido cluster complexes have attracted attention because of possible synergistic effects [3] exhibited by certain types of heterogeneous metal sulfide catalysts [4].

Insertion of a metal group into the sulfur–sulfur bond of complexes containing the disulfido ligand is a convenient route for the synthesis of heteronuclear metal complexes with sulfido ligands [5]. Recently, we have reported the disulfido complexes $Mn_2(CO)_7(\mu\text{-}S_2)$ [6] and $CpMoMn(CO)_5(\mu\text{-}S_2)$ [7]. These complexes exhibit facile insertions of metal containing fragments into the S–S bond of the disulfido ligand to yield mixed metal cluster complexes containing two triply bridging sulfido ligands, Eqs. (1) and (2) [5a,5b,8].

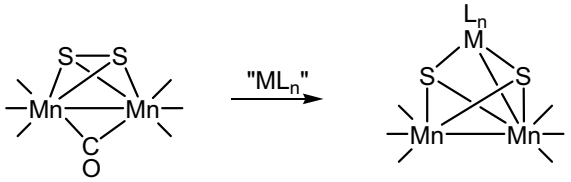

(1)

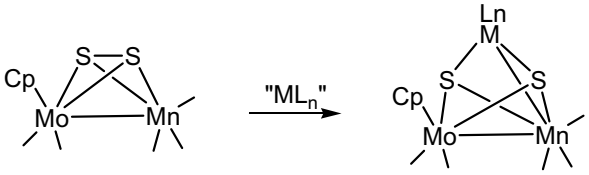

Only a few mixed metal carbonyl complexes containing disulfido ligands have been reported [7]. We have now investigated the room temperature reaction of $[CpFeMn(CO)_5(\mu_3\text{-}S_2)]_2$ (**1**) with CO in the presence of light [9].

* Corresponding author.
E-mail address: Adams@mail.chem.sc.edu (R.D. Adams).
[1] Present address: Department of Chemistry, University of Miami, Coral Gables, FL 33146, United States.
[2] Present address: Department of Chemistry, The University of Memphis, Memphis, TN 38138, United States.

0022-328X/$ - see front matter © 2008 Elsevier B.V. All rights reserved.
doi:10.1016/j.jorganchem.2008.05.029

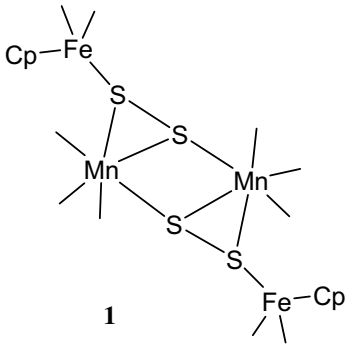

1

Two mixed metal complexes $CpFeMn_2(CO)_7(\mu_3\text{-}S_2)_2$ (**2**) and $Cp_3Fe_3Mn(CO)_4(\mu_3\text{-}S_2)_2(\mu_3\text{-}S)$ (**3**) were obtained. Both have been characterized crystallographically. The major product **2** is paramagnetic and has been studied by a combination of EPR, magnetic susceptibility, cyclic voltammetry and computational analyses. The results of these studies are reported herein.

2. Experimental

2.1. General data

All reactions were performed under a nitrogen atmosphere using Schlenk techniques. Reagent grade solvents were dried by the standard procedures and were freshly distilled prior to use. Infrared spectra were recorded on a Thermo-Nicolet Avatar 360 FTIR spectrophotometer. Electrospray mass spectrometric measurements were obtained on a MicroMass Q-Tof spectrometer. Elemental analyses were performed by Desert Analytics (Tucson, AZ). $[CpFeMn(CO)_5(\mu_3\text{-}S_2)]_2$ was prepared by the published procedure [9]. Unless stated otherwise, all product isolations were performed by TLC in air on Analtech 0.25 and 0.5 mm silica gel 60 Å F_{254} glass plates.

2.2. Reaction of $[CpFeMn(CO)_5(\mu_3\text{-}S_2)]_2$ (**1**) with CO

A solution of **1** (25 mg, 0.0329 mmol) in CH_2Cl_2 (10 mL) was stirred under CO atmosphere at room temperature in the presence of room light for 36 h. Note: No product was obtained when the reaction was performed in the dark. The solvent was then removed *in vacuo* and the residue was separated by TLC on silica gel using 1:1 hexane/CH_2Cl_2 solvent mixture to yield in order of elution 7.5 mg (41%) of brown–green $CpFeMn_2(CO)_7(\mu_3\text{-}S_2)_2$ (**2**) and 1.1 mg (5%) of $Cp_3Fe_3Mn(CO)_4(\mu_3\text{-}S_2)_2(\mu_3\text{-}S)$ (**3**). The known compound $[CpFe(CO)_2]_2$ can subsequently be eluted from the baseline in approx. 20% yield by using pure CH_2Cl_2 elution solvent [10,11]. Spectral data for **2**: IR ν_{CO} (cm^{-1} in CH_2Cl_2) 2088(m), 2021(vs), 2010(s), 1972(m), 1951(m), 1932(m). Anal. Calc. for $C_{12}H_5FeMn_2O_7S_4$: C, 25.96; H, 0.91. Found: C, 25.62; H, 0.97%. Spectral data for **3**: IR ν_{CO} (cm^{-1} in CH_2Cl_2) 2003(s), 1925(m), 1769(vw). ^1H NMR (in $CDCl_3$): $\delta = 4.94$ (s, 10H, Cp), 4.70 (s, 5H, Cp). MS (*e*/*z*): 691 (M+H).

2.3. Electrochemical measurements

Cyclic voltammetric experiments were conducted by using a CV-50W voltammetric analyzer purchased from Bioanalytical Systems, West Lafayette, IN. The experiments were done under a nitrogen atmosphere at room temperature in 10.0 mL of CH_3CN solution by using 1.0 mM solutions of compound **2** with 0.1 mol/L tetrabutylammonium hexafluorophosphate as the supporting electrolyte. Cyclic voltammograms (CVs) were obtained by using a three-electrode system consisting of a platinum working electrode, a platinum counter and an Ag/AgCl reference electrode. Half-wave potentials ($E_{1/2}$) were calculated as the mean potential between the peak potential by use of the equation $E_{1/2} = (E_{pa} + E_{pc})/2$, where E_{pa} is the anodic peak potential and E_{pc} is the cathodic peak potential.

2.4. EPR measurements

Q-band (~34 GHz) EPR measurements were performed on samples dissolved in benzene on a Bruker E500 spectrometer. The magnetic field was calibrated with a built-in NMR teslameter and the frequency was recorded using a digital frequency counter. The temperature was varied between 300 and 4 K using a continuous flow liquid He cryostat. The measurements of $FeMn_2$ were made in benzene solutions, as a frozen glass, and also in a powder form.

2.5. Magnetic susceptibility measurements

Magnetic susceptibility experiments were carried out under a 100 Gauss magnetic field on powder samples of **2** using a Quantum Design MPMS XL SQUID Magnetometer. The temperature range was 1.8–200 K within an accuracy of 0.05 K.

2.6. Crystallographic analysis

Dark brown crystals of **2** suitable for diffraction analysis were obtained by slow evaporation of solvent from solutions in hexane/methylene chloride solvent mixtures at −20 °C. Brown crystals of **3** were grown from benzene/octane solvent mixture at 5 °C. Each data crystal was glued onto the end of a thin glass fiber. X-ray intensity data were measured by using a Bruker SMART APEX CCD-based diffractometer using Mo Kα radiation ($\lambda = 0.71073$ Å). The unit cells were initially determined based on reflections selected from a set of three scans measured in orthogonal wedges of reciprocal space. The raw data frames were integrated with the SAINT+ program using a narrow-frame integration algorithm [12]. Corrections for the Lorentz and polarization effects were also

Table 1
Crystallographic data for compounds **2** and **3**

Compound	**2**	**3**
Empirical formula	$C_{12}H_5FeMn_2O_7S_4$	$C_{19}H_{15}Fe_3MnO_4S_5$
Formula weight	555.13	690.10
Crystal system	Orthorhombic	Orthorhombic
Space group	*Pbca*	*Pnma*
a (Å)	11.6750(8)	9.6752(6)
b (Å)	10.3065(6)	13.2698(9)
c (Å)	30.3598(9)	17.8969(12)
$\alpha = \beta = \gamma$ (°)	90	90
V (Å^3)	3653.1(3)	2297.7(3)
Z	8	4
T (K)	296(2)	291(2)
ρ_{calc} (g/cm^3)	2.019	1.995
μ (Mo Kα) (mm^{-1})	2.634	2.874
Number of observations ($I > 2\sigma(I)$)	2717	1956
Number of parameters	230	150
Goodness-of-fit[a]	1.062	1.014
Maximum shift in final cycle	0.001	0.001
Residuals: R_1; wR_2[b]	0.0459; 0.0906	0.0451; 0.0997
Absorption Correction, maximum/minimum	1.000/0.877	1.000/0.866
Largest peak in difference map (e$^-$/Å^3)	0.735	0.630

[a] $GOF = [\Sigma_{hkl}(w(|F_{obs}^2| - |F_{calc}^2|))^2/(n_{data} - n_{vari})]^{1/2}$.
[b] $R_1 = \Sigma(||F_{obs}| - |F_{calc}||)/\Sigma|F_{obs}|$. $wR_2 = \{\Sigma[w(|F_{obs}^2 - F_{calc}^2|)^2/\Sigma[w(F_{obs}^2)^2]\}^{1/2}$; $w = 1/\sigma^2(F_{obs}^2)$.

applied by using the program SAINT. An empirical absorption correction based on the multiple measurement of equivalent reflections was applied for each analysis by using the program SADABS. Crystal data, data collection parameters, and results of the analyses are listed in Table 1. The structures were solved by a combination of direct methods and difference Fourier syntheses. All non-hydrogen atoms were refined with anisotropic thermal parameters. The positions of the hydrogen atoms were calculated by assuming idealized geometries and were refined by using the riding model. Refinements were carried out on F^2 by the method of full-matrix least-squares by using the SHELXTL program library with neutral atom scattering factors [13].

Compounds **2** and **3** both crystallized in the orthorhombic crystal system. The space group *Pbca* identified uniquely for **2** on the basis of the systematic absences observed in the data. The systematic absences for **3** were consistent with either of the space groups *Pnma* and $Pna2_1$. The centrosymetrical one was tested first and confirmed by the successful solution and refinement of the structure. For both compounds, the cyclopentadienyl groups were disordered equally over two sites. These carbon atoms were refined with isotropic displacement parameters.

2.6.1. Computational treatments

Density functional theory (DFT) calculations were performed using the GAUSSIAN03 suite of programs [14]. Unrestricted and restricted open-shell single point calculations were conducted using the Becke3 exchange functional [15], in combination with the Lee, Yang, and Parr correlation functional [16], i.e. the B3LYP method, as implemented in GAUSSIAN03. The positions of the heavy atoms were taken from the X-ray crystallographic analysis and all C–H bond distances were adjusted to 1.09 Å. The basis set used for unrestricted and restricted open-shell single point calculations was as follows: modified valence double-zeta LANL2DZ [17] basis sets with a sets of 4p functions developed by Couty and Hall were used for iron and manganese [18]. The LANL2DZ basis set and accompanying ECP was employed for sulfur, while D95V basis sets were used for hydrogen, carbon, and oxygen [19]. The representations of the molecular orbitals were visualized using the JIMP software program[20]. Fenske-Hall (FH) calculations [21] were performed utilizing a graphical user interface developed [20] to build inputs and view outputs from stand-alone Fenske-Hall (Version 0.1.v117) and MOPLOT2 [22] binary executables. Contracted double-ζ basis sets were used for the Fe 3d, Mn 3d, and for the C and O 2p atomic orbitals. The Fenske-Hall scheme is a non-empirical, approximate method that is capable of calculating molecular orbitals that are usually quite similar to those from DFT [21b] for transition metal systems and has built-in fragment analysis routines that also allow one to assemble transition metal cluster structures from the ligand containing fragments.

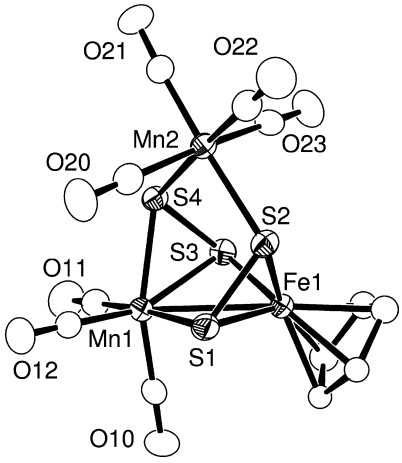

Fig. 1. An ORTEP diagram of the molecular structure of compound **2**, showing 40% thermal ellipsoid probabilities.

3. Results

Two new compounds $CpFeMn_2(CO)_7(\mu_3\text{-}S_2)_2$ (**2**) (41% yield) and $Cp_3Fe_3Mn(CO)_4(\mu_3\text{-}S_2)_2(\mu_3\text{-}S)$ (**3**) (5% yield) were obtained from the reaction of **1** with CO at room temperature in the presence of room light. The products were not obtained when a solution of **1** under a CO atmosphere was maintained in the dark. The molecular structure of **2** was established by a single crystal X-ray diffraction analysis. An ORTEP diagram of its molecular structure is shown in Fig. 1. Selected bond distances and angles are listed in Table 2. Compound **2** contains two manganese atoms and only one iron atom. There are two triply bridging disulfido ligands, S(1)–S(2) and S(3)–S(4), but each disulfido ligand has four metal–sulfur bonds. This is because in both cases both sulfur atoms in the disulfido ligand are bond to a common metal atom; for S(1)–S(2) this is Fe(1), Fe(1)–S(1) = 2.2446(14) Å, Fe(1)–S(2) = 2.2583(13) Å, while for S(3)–S(4) this is Mn(1), Mn(1)–S(3) = 2.3678(14) Å, Mn(1)–S(4) = 2.3631(13) Å. Note: the Mn–S bonds are significantly longer than the Fe–S bonds. The distances between Fe and S, 2.1942(13) Å and 2.2446(14) Å, are shorter than that in **1** [9]. In spite of this unusual coordination, the S–S bond distances are normal, S(1)–S(2) = 2.0574(17) Å and S(3)–S(4) = 2.0859(16) Å and similar to that found in **1**, 2.0740(8) Å. There is only one significant metal–metal interaction, Fe(1)–Mn(1) = 2.9550(9) Å. Whether this is a full bond or not could be debated. The bond is significantly longer than the Fe–Mn single bond distances observed for the compounds $Cp(CO)_2FeMn(CO)_5$, 2.843(4) Å [23] and $Cp(CO)_2FeMn(CO)_4(CNBu^t)$, 2.841(1) Å [24], but is certainly short enough to permit a significant orbital overlap, see below.

Assuming the bridging disulfido ligands serve as neutral six-electron donors, compound **2** should contain an odd number of electrons, a total of 53 valence electrons. A three metal cluster with one metal–metal bond should have 52 valence electrons if all of the metal atoms have 18 electron configurations. This compound exceeds that number by one electron, so one of the metal atoms must be considered to have a formal "19" electron configuration.

Table 2
Selected intramolecular bond distances and angles for **2**[a]

Atom	Atom	Distance (Å)	Atom	Atom	Distance (Å)
(a) Distances					
Mn(1)	Fe(1)	2.9550(9)	Fe(1)	S(3)	2.1942(13)
Mn(1)	S(1)	2.3470(15)	Fe(1)	S(2)	2.2583(13)
Mn(1)	S(4)	2.3631(13)	Fe(1)	S(1)	2.2446(14)
Mn(1)	S(3)	2.3678(14)	S(1)	S(2)	2.0574(17)
Mn(2)	S(2)	2.3417(13)	S(3)	S(4)	2.0859(16)
Mn(2)	S(4)	2.3562(13)	C	O	1.136(6)(av)

Atom	Atom	Atom	Angle (°)	Atom	Atom	Atom	Angle (°)
(b) Angles							
S(1)	Mn(1)	S(4)	94.52(5)	S(2)	S(1)	Mn(1)	109.38(6)
S(1)	Mn(1)	S(3)	90.94(5)	Fe(1)	S(1)	Mn(1)	80.08(5)
S(4)	Mn(1)	S(3)	52.32(4)	S(1)	S(2)	Fe(1)	62.47(5)
S(1)	Mn(1)	Fe(1)	48.44(3)	S(1)	S(2)	Mn(2) Mn(2)	111.28(6)
S(4)	Mn(1)	Fe(1)	81.71(4)	Fe(1)	S(2)	Fe(1)	116.74(5)
S(3)	Mn(1)	Fe(1)	47.11(3)	S(4)	S(3)	Mn(1)	110.04(6)
S(2)	Mn(2)	S(4)	89.60(5)	S(4)	S(3)	Mn(1)	63.72(5)
S(3)	Fe(1)	S(1)	98.43(5)	Fe(1)	S(3)	Mn(2)	80.64(5)
S(2)	S(1)	Fe(1)	63.15(5)	S(3)	S(4)	Mn(1)	108.34(6)
S(3)	S(4)	Mn(1)	63.96(5)	Mn(2)	S(4)		116.61(5)

[a] Estimated standard deviations in the least significant figure are given in parentheses.

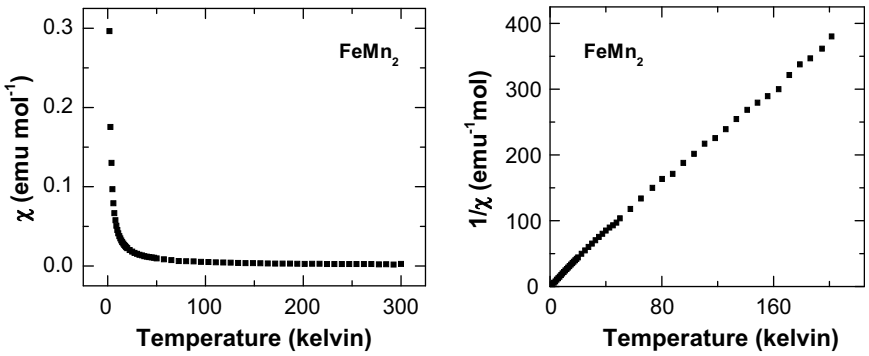

Fig. 2. χ vs. T (left) and $1/\chi$ vs. T (right) plots of the magnetic susceptibility of compound **2** in the solid state.

The magnetic susceptibility of compound **2** in the solid state exhibits a simple paramagnetic behavior and confirms the presence of one unpaired electron per formula unit, see Fig. 2. Accordingly, no resonance was observed for the protons on the cyclopentadienyl ligand in its ^{1}H NMR spectrum. Because of its anomalous electron configuration, a computational analysis of **2** was performed in order to obtain a clearer picture of its bonding.

3.1. Computational analysis of **2**

DFT calculations were performed in order to understand the bonding in the complex and to try to define the character of the orbital that contains the unpaired electron. Restricted open-shell B3LYP (ROB3LYP) calculations predict a doublet ground state for the complex. The calculation indicates that 77.4% of the spin density from the unpaired electron is located on the Fe atom. The next highest contributions to the spin density are located on the S atoms (6.4% and 4.8%) that bridge the Fe and Mn atoms, followed by the manganese atom Mn(1) (3.5%) in the bottom left of Fig. 3. The residual spin density is distributed among the remaining atoms in the complex, with no more than 1.4% of the spin density on any other atom. The unrestricted B3LYP calculation also predicts that the majority of the spin density is located on the Fe atom.

Visual representations of a singly-occupied molecular orbital (SOMO) that were generated from the restricted open-shell calculation are consistent with the assignment of unpaired spin density primarily to the Fe atom. As shown in Figs. 3 and 4, the SOMO is primarily a mixture of Fe d orbitals, with small contributions from the bridging S atoms and the Mn atom in the bottom left of Fig. 3 The SOMO contains a slight anti-bonding interaction between the Fe and Mn atom (Figs. 3 and 4). This small anti-bonding interaction causes the SOMO to be higher in energy than the two other fully occupied d orbitals on the Fe (low spin d^5) and the three other fully occupied d orbitals on each of the Mn atoms (low spin d^6) that do not have unfavorable metal–metal anti-bonding interactions. Unfortunately, due to extensive orbital mixing caused by the low symmetry of this complex, the restricted open-shell B3LYP calculation did not generate a complementary molecular orbital that clearly contained the bonding combination of the Fe and Mn d orbitals interacting in the SOMO. However, Fenske-Hall calculations on the complex were successful in generating both a similar SOMO (Fig. 5) and a molecular orbital that shows a bonding interaction between d orbitals from the Fe and Mn (Fig. 6). In agreement with the restricted open-shell B3LYP calculations, Fenske-Hall calculations predict an anti-bonding interaction between the Fe and Mn, with Fe as the major contributor (49.6%) to the SOMO

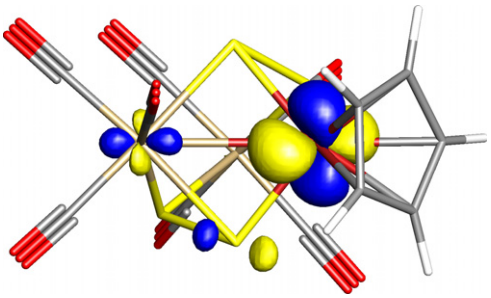

Fig. 4. The SOMO generated from the restricted open-shell B3LYP calculation rotated ~90° from the view in Fig. 1 with an isodensity value of 0.065. This view highlights the slight Fe–Mn anti-bonding character in the SOMO.

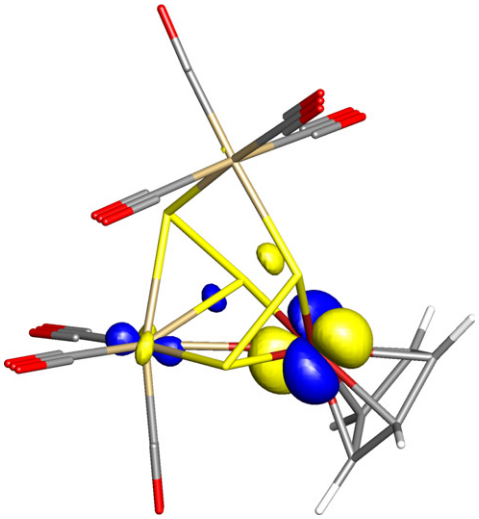

Fig. 3. The SOMO generated from the restricted open-shell B3LYP calculation with an isodensity value of 0.065.

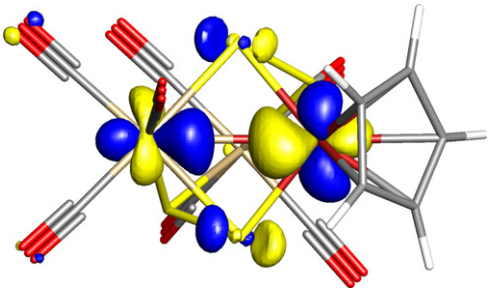

Fig. 5. The SOMO generated from the Fenske-Hall calculations with an isodensity value of 0.065.

and with the next largest contributions coming from Mn (22.7%) and the bridging S atoms (6.7% and 6.3%). Fenske-Hall calculations also predict a complimentary Fe–Mn bonding orbital containing approximately equal contributions from the Fe (32.2%) and the Mn (32.1%) (Fig. 6). Due to this favorable Fe–Mn bonding interaction, the orbital in Fig. 6 has the lowest energy of all of the occupied valence d orbitals. Since the anti-bonding SOMO only contains one electron, Fenske-Hall calculations indicate that there is a net 1 electron bond between the Fe and Mn. However, it should be noted that both the restricted open-shell and unrestricted B3LYP calculations indicate low spin density on Mn, which suggests that the Fe–Mn bonding interaction may be weaker than is predicted by the Fenske-Hall calculation.

A number of resonance structures could be imagined in order to rationalize the bonding in **2** as described above. Two of these are shown in Fig. 7. In structure **A**, it is assumed that there is an Fe–Mn bond involving atom Mn(1). In this structure the Fe atom has a 19 electron configuration. This description is consistent with the Fenske-Hall model described above. In structure **B**, it is assumed that there is no Fe–Mn bond and the Fe atom has a 17 electron configuration. In both structures there is an unpaired electron on the Fe atom.

3.1.1. EPR measurements

EPR measurements were performed in order to establish further the nature of the orbital in **2** that contains the unpaired electron. Fig. 8 shows the EPR spectra of **2** in a solution in benzene at 295 K and in a frozen glass at 20 K. The Lande *g* tensor components for **2** are given in Table 3. The spectra of both isotropic solution samples (295 K) and the frozen glass (20 K) are devoid of any hyperfine structure, Fig. 8a. The room temperature spectrum consists of a single featureless peak. There is a small, likely unrelated component, present at higher fields (labeled g^*). Upon freezing, the low-field peak splits into the three *g*-tensor components expected for a low symmetry system. The sharp contribution in the frozen glass spectrum is most likely related to the g^* peak observed at room temperature. Similarly, the powder spectrum, Fig. 8b, shows evidence of ^{55}Mn hyperfine structure only near $g = 2$, which is also attributed to a small amount of impurity or decomposition product.

Because no characteristic hyperfine structure is evident for either species, we cannot unequivocally assign localization of the unpaired spin to a Mn or Fe ion, but from the solution phase EPR line widths, we can state that the upper limit on the Mn hyperfine

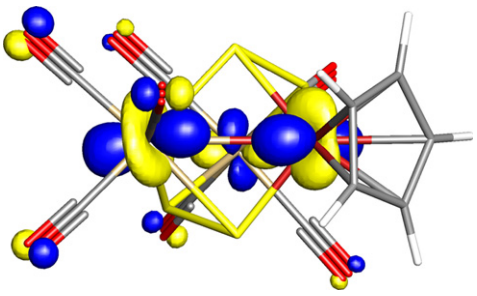

Fig. 6. A JIMP representation of Fe–Mn bonding orbital generated from Fenske-Hall calculations with an isodensity value of 0.065.

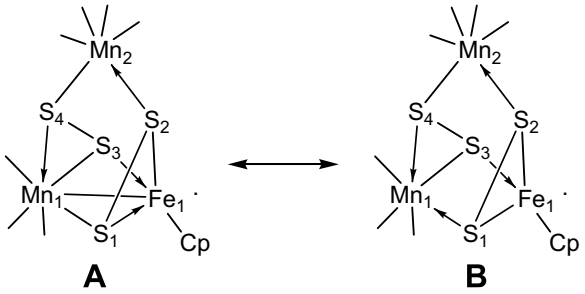

Fig. 7. Two resonance structures to explain the bonding in **2**. In (A) the Fe atom has a 19 electron configuration. In (B) the Fe atom has a 17 electron configuration.

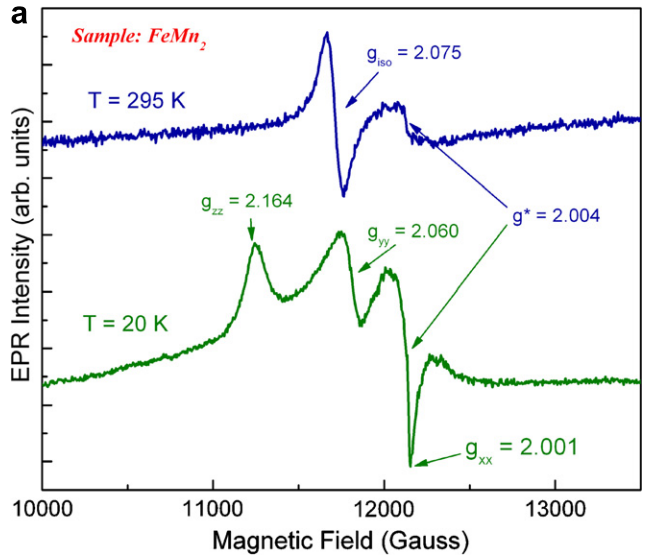

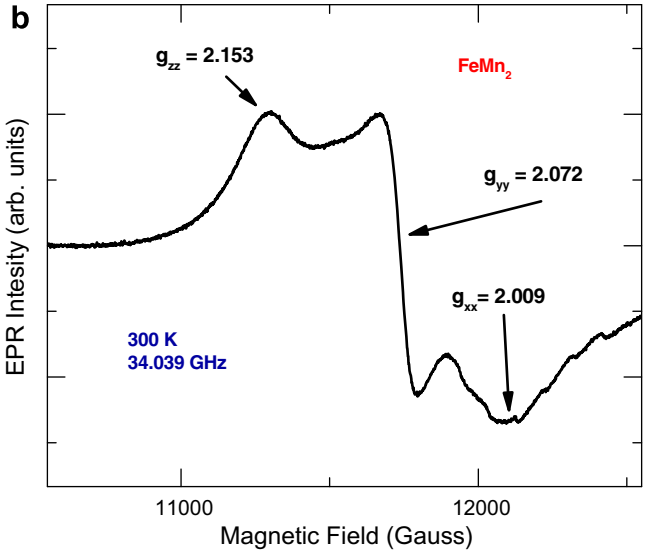

Fig. 8. Q-band (34 GHz) EPR spectra of **2**: (a) in benzene at 295 K and in a frozen glass at 20 K (b) powder sample.

Table 3
Lande *g* tensor components compound **2**

Compound	g_{iso}	g_{xx}	g_{yy}	g_{zz}
$FeMn_2$ (solution)	2.075			
$FeMn_2$[a] (Frozen glass)	2.075*	2.001	2.060	2.164
$FeMn_2$ powder (300 K)	2.078*	2.009	2.072	2.153

[a] Values marked with an asterisk correspond to a calculated value ($g_{iso} = 1/3 (g_{xx} + g_{yy} + g_{zz})$).

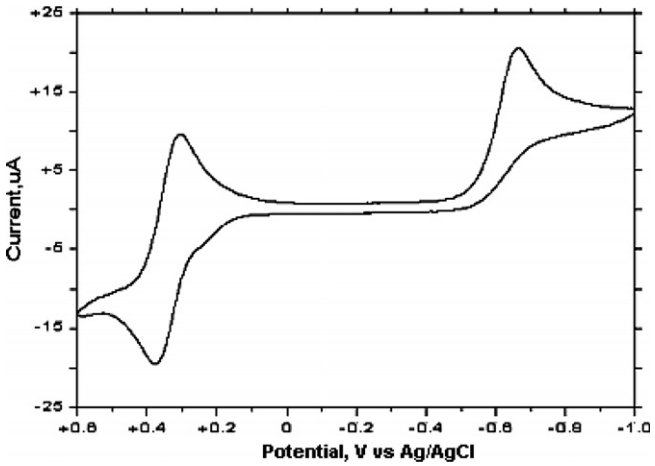

Fig. 9. CV trace of compound **2** (1.0 mmol/L) in CH_3CN (10 mL) with $[Bu^n_4N]PF_6$ (0.1 mol/L).

constant is 3.4 Gauss, which puts an upper limit of less than 5% of the unpaired electron spin density on the Mn atom. On the other hand, the *g*-anisotropy ranging from about 2.00 to 2.16 points strongly toward the spin density being localized on metal-based orbitals rather than ligand orbitals. The unpaired electron is thus seen to be at least 95% localized on the Fe atom, essentially in agreement with the theoretical predictions.

3.1.2. Cyclic voltammetry

The electrochemical properties of compound **2** were measured by cyclic voltammetry in acetonitrile by using tetrabutylammonium hexafluorophosphate as the supporting electrolyte. The cyclic voltammogram of **2** is shown in Fig. 9. One well-defined reversible one-electron wave was found at +0.34 V. This is attributed a reversible oxidation of the complex and formation of a monocation. Presumably, this oxidation corresponds to the removal of the unpaired electron from the SOMO of **2** that is shown in Figs. 3 and 4. Attempts to produce this oxidation chemically in order to isolate and characterize the cation were unsuccessful. In addition there is an irreversible one-electron wave at −0.66 V vs. Ag/AgCl that is attributed to reduction to an unstable monoanion. This reduction probably corresponds to the addition of an electron to the SOMO of **2**. Attempts to isolate this unstable anion were also unsuccessful.

Compound **3** is a minor coproduct from this reaction. Compound **3** was characterized crystallographically and an ORTEP

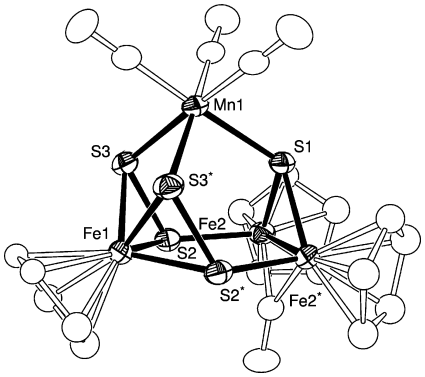

Fig. 10. An ORTEP diagram of the molecular structure of compound **3** showing 50% thermal ellipsoid probabilities.

Table 4
Selected intramolecular bond distances and angles for **3**[a]

Atom	Atom	Distance (Å)	Atom	Atom	Distance (Å)
(a) Distances					
Fe(1)	S(2)	2.293(1)	Mn(1)	S(1)	2.3706(16)
Fe(1)	S(3)	2.2858(12)	Mn(1)	S(3)	2.3218(12)
Fe(2)	Fe(2*)	2.545(1)	S(2)	S(3)	2.0711(14)
Fe(2)	S(1)	2.2119(12)	C	O	1.15(1)(av)
Fe(2)	S(2)	2.1575(13)			

Atom	Atom	Atom	Angle (°)	Atom	Atom	Atom	Angle (°)
(b) Angles							
S(3*)	Fe(1)	S(3)	82.83(6)	Fe(2)	S(1)	Fe(2*)	70.24(5)
S(3)	Mn(1)	S(1)	93.54(4)	Fe(2)	S(1)	Mn(1)	118.33(6)
Fe(2)	S(2)	Fe(1)	122.84(5)	S(3)	S(2)	Fe(2)	115.80(6)
Fe(1)	S(3)	Mn(1)	96.18(4)	S(2)	S(3)	Fe(1)	63.29(4)
S(3)	S(2)	Fe(1)	62.93(5)	S(2)	S(3)	Mn(1)	109.76(6)

[a] Estimated standard deviations in the least significant figure are given in parentheses.

diagram of its molecular structure is shown in Fig. 10. Selected bond distances and angles are listed in Table 4. The molecule contains a crystallographically-imposed reflection plane. The compound contains three iron atoms and only one manganese atom. Each iron atom contains one C_5H_5 ligand. The manganese atom contains three linear terminal carbonyl ligands. There are two triply bridging disulfido ligands, S(2)–S(3) and S(2*)–S(3*) and one mono-sulfido ligand S(1). Atoms Fe(1), Mn(1) and S(1) lie on the reflection plane. Fe(1) is bonded to all four sulfur atoms of the bridging disulfido ligands, Fe(1)–S(2) = 2.293(1) Å and Fe(1)–S(3) = 2.2858(12) Å. These distances are slightly longer, probably for steric reasons, than the Fe–S distances in **2** which is bonded to only three sulfur atoms. A similarly coordinated iron atom was found in the complex, $(MeCp)_2Fe_2(CO)(\mu\text{-}S_2)_2$ (**4**) [25]. The Fe(2)–Fe(2*) distance is quite short and clearly indicative of an Fe–Fe bonding interaction. The Fe(2)–Fe(2*) distance of 2.545(1) Å and is very similar to the Fe–Fe distance in $[CpFe(CO)_2]_2$, *cis*-isomer, 2.531(1) Å [10]; *trans*-isomer, 2.534(2) Å [11]. The S(2)–S(3) bond distance 2.0711(14) Å is quite similar to the S–S bond distances observed in compounds **1** and **2**. Compound **3** is diamagnetic; all four metal atoms have 18 electron configurations, and the ^1H NMR spectrum of **3** exhibits two singlets: δ = 4.94 (10H) and 4.70 (5H) for the cyclopentadienyl ligands.

4. Discussion

In previous studies we have shown that the compound **1** spontaneously condenses to form a higher nuclearity species upon mild heating in which the disulfide ligands have adopted a greater degree of bridging coordination to the metal atoms [9]. In this work we have shown that in the presence of light and CO, compound **1** is degraded to form new polynuclear mixed metal species: one of lower nuclearity **2** and one species of same nuclearity, but a different combination of the metal atoms **3**. Scheme 1 shows a possible transformation of **1**–**2**. A homolytic cleavage of one of the $CpFe(CO)_2$ groups from one of the disulfido ligands induced by irradiation could yield a radical intermediate such as **C** on the sulfur atom S(3). A subsequent shift of one CO ligand from Fe(1) to Mn(2), formation of bonds between Fe(1) and S(1) and S(3), and the loss of a CO ligand from Fe(1) would complete the formation of **2**. As in the previous study of **1** [9], the disulfido ligands adopt higher bridging coordinations in the formation of **2**. The formation of $[CpFe(CO)_2]_2$ as a coproduct is explained as a combination of two $CpFe(CO)_2$ groups from the homolytic cleavage from **1**.

The formation of **3** is more difficult to explain. Suffice it to say, the generation of CpFe fragments would be expected to permit the

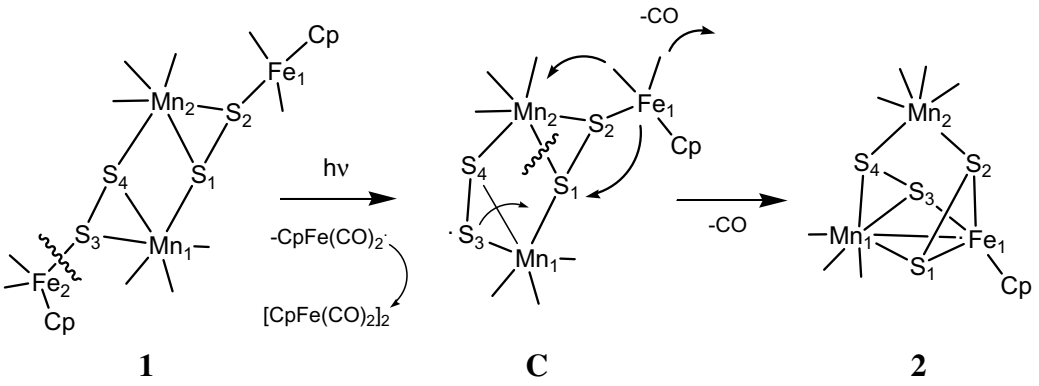

1 C 2

Scheme 1.

formation of iron-rich containing disulfido cluster complexes such as **3** by further reactions with **1**.

Acknowledgements

This research was supported by Grants from the National Science Foundation, Grant Nos. CHE-9909017, CHE-0518074 and CHE-0541587, NIRT/DMR 0506946, and the Welch Foundation (A-648). We thank Dr. Matthew Davis for making the magnetic susceptibility measurements.

Appendix A. Supplementary material

CCDC 688156 and 688157 contain the supplementary crystallographic data for compounds **2** and **3**. These data can be obtained free of charge from The Cambridge Crystallographic Data Centre via www.ccdc.cam.ac.uk/data_request/cif. Supplementary data associated with this article can be found, in the online version, at doi:10.1016/j.jorganchem.2008.05.029.

References

[1] (a) S. Dehnen, A. Eichhofer, D. Fenske, Eur. J. Inorg. Chem. (2002) 279–288;
(b) T. Shibahara, Coord. Chem. Rev. 123 (1993) 73–147;
(c) K.H. Whitmire, J. Coord. Chem. 17 (1988) 95–203;
(d) R.D. Adams, M. Tasi, J. Cluster Sci. 1 (1990) 249–267;
(e) R.D. Adams, Polyhedron 4 (1985) 2003–2025.
[2] (a) J. Wachter, Angew. Chem., Int. Ed. Engl. 28 (1989) 1613–1626;
(b) R.B. King, T.E. Bitterwolf, Coord. Chem. Rev. 206–207 (2000) 563–579;
(c) K.H. Witmire, in: G. Wilkinson, F.G.A. Stone, E. Abel (Eds.), Comprehensive Organometallic Chemistry II, vol. 7, Pergamon Press, New York, 1995 (Chapter 1), sec. 1.11.2.2, p. 62 and references therein.
[3] M. Boudart, J.S. Arrieta, R. Dallabetta, J. Am. Chem. Soc. 105 (1983) 6501–6502. and references therein.
[4] (a) M. Hidai, S. Kuwata, Y. Mizobe, Accts. Chem. Res. 33 (2000) 46–52;
(b) M.A. Casado, M.A. Ciriano, A.J. Edwards, F.J. Lahoz, J.J. Perez-Torrente, L.A. Oro, Organometallics 17 (1998) 3414–3416;
(c) C.J. Ruffing, R.B. Rauchfuss, Organometallics 4 (1985) 524–528;
(d) S.H. Pawlicki, B.C. Noll, M. Rakowski DuBois, J. Coord. Chem. 56 (2003) 41–47.
[5] (a) R.D. Adams, O.S. Kwon, M.D. Smith, Organometallics 21 (2002) 1960–1965;
(b) R.D. Adams, O.S. Kwon, M.D. Smith, Inorg. Chem. 41 (2002) 1658–1661;
(c) D. Seyforth, R.S. Henderson, L.-C. Song, Organometallics 1 (1982) 125–133;
(d) M.J. Don, M.G. Richmond, Inorg. Chim. Acta 210 (1993) 129–130;
(e) M. Cowie, R.L. Dekock, T.R. Wagenmaker, D. Seyforth, R.S. Henderson, M.K. Gallagher, Organometallics 8 (1989) 119–132;
(f) V.W. Day, D.A. Lesch, R.B. Rauchfuss, J. Am. Chem. Soc. 104 (1982) 1290–1295;
(g) M.D. Curtis, P.D. Williams, W.M. Butler, Inorg. Chem. 27 (1988) 2853–2862.
[6] R.D. Adams, O.S. Kwon, M.D. Smith, Inorg. Chem. 41 (2002) 6281–6290.
[7] (a) R.D. Adams, O.S. Kwon, S. Miao, Accts. Chem. Res. 38 (2005) 183–190;
(b) R.D. Adams, O.S. Kwon, S. Miao, Inorg. Chem. 42 (2003) 3356–3365.
[8] R.D. Adams, S. Miao, Organometallics 22 (2003) 2492–2497.
[9] R.D. Adams, B. Captain, O.-S. Kwon, P.J. Pellechia, S. Sanyal, J. Organomet. Chem. 689 (2004) 1370–1376.
[10] R.F. Bryan, P.T. Greene, M.J. Newlands, D.S. Field, J. Chem. Soc. A (1968) 3068–3074.
[11] R.F. Bryan, P.T. Greene, J. Chem. Soc. A (1968) 3064–3068.
[12] SAINT+, Version 6.02a; Bruker Analytical X-ray Systems Inc., Madison, WI, 1998.
[13] G.M. Sheldrick, SHELXTL, Version 5.1; Bruker Analytical X-ray Systems Inc., Madison, WI, 1997.
[14] GAUSSIAN03, Revision B.05: M.J. Frisch, G.W. Trucks, H.B. Schlegel, G.E. Scuseria, M.A. Robb, J.R. Cheeseman, J.A. Montgomery, Jr., T. Vreven, K.N. Kudin, J.C. Burant, J.M. Millam, S.S. Iyengar, J. Tomasi, V. Barone, B. Mennucci, M. Cossi, G. Scalmani, N. Rega, G.A. Petersson, H. Nakatsuji, M. Hada, M. Ehara, K. Toyota, R. Fukuda, J. Hasegawa, M. Ishida, T. Nakajima, Y. Honda, O. Kitao, H. Nakai, M. Klene, X. Li, J.E. Knox, H.P. Hratchian, J.B. Cross, V. Bakken, C. Adamo, J. Jaramillo, R. Gomperts, R.E. Stratmann, O. Yazyev, A.J. Austin, R. Cammi, C. Pomelli, J.W. Ochterski, P.Y. Ayala, K. Morokuma, G.A. Voth, P. Salvador, J.J. Dannenberg, V.G. Zakrzewski, S. Dapprick, A.D. Daniels, M.C. Strain, O. Farkas, D.K Malick, A.D. Rabuck, K. Raghavachari, J.B. Foresman, J.V. Ortiz, Q. Cui, A.G. Baboul, S. Clifford, J. Cioslowski, B.B. Stefanov, G. Liu, A. Liashenko, P. Piskorz, I. Komaromi, R.L. Martin, D.J. Fox, T. Keith, M.A. Al-Laham, C.Y. Peng, A. Ananyakkara, M. Challacombe, P.M.W. Gill, B. Johnson, W. Chen, M.W. Wong, C. Gonzalex, J.A. Pople, Gaussian Inc., Wallingfort, CT, 2004.
[15] A.D. Becke, J. Chem. Phys. 98 (1993) 5648–5652.
[16] C. Lee, W. Yang, R.G. Parr, Phys. Rev. B. 37 (1988) 785–789.
[17] (a) P.J. Hay, W.R. Wadt, J. Chem. Phys. 82 (1985) 270–283;
(b) W.R. Wadt, P.J. Hay, J. Chem. Phys. 82 (1985) 284–298;
(c) P.J. Hay, W.R. Wadt, J. Chem. Phys. 82 (1985) 299–310.
[18] M. Couty, M.B. Hall, J. Comput. Chem. 17 (1996) 1359–1370.
[19] T.H. Dunning, P.J. Hay, in: H.D. Schaefer III (Ed.), Modern Theoretical Chemistry, Plenum, New York, 1976, pp. 1–28.
[20] M. Manson, C.E. Webster, M.B. Hall, JIMP Development Version 0.1 (built for Windows PC and Redhat Linux 7.3); Department of Chemistry, Texas A&M University, College Station, TX 77842 (http://www.chem.tamu.edu/jimp/).
[21] (a) M.B. Hall, R.F. Fenske, Inorg. Chem. 11 (1972) 768–775;
(b) C.E. Webster, M.B. Hall, in: C. Dykstra (Ed.), Theory and Applications of Computational Chemistry: The First Forty Years, Elsevier, Amsterdam, 2005, pp. 1143–1165 (Chapter 40).
[22] MOPLOT2: for orbital and density plots from linear combinations of Slater or Gaussian type orbitals; Version 2.0, June 1993; D.L. Lichtenberger, Department of Chemistry, University of Arizona, Tucson, AZ 85721.
[23] P.J. Hensen, R.A. Jacobson, J. Organomet. Chem. 6 (1966) 389–398.
[24] P. Johnston, G.J. Hutchings, L. Denner, J.C.A. Boeyens, N.J. Coville, Organometallics 6 (1987) 1292–1300.
[25] C. Giannotti, A.M. Ducourant, H. Chanaud, A. Chiaroni, C. Riche, J. Organomet. Chem. 140 (1977) 289–295.